

The desmoplakin–intermediate filament linkage regulates cell mechanics

Joshua A. Broussard^{a,b,†}, Ruiguo Yang^{c,†,‡}, Changjin Huang^{c,§}, S. Shiva P. Nathamgari^c, Allison M. Beese^{c,||}, Lisa M. Godsel^{a,b}, Marihan H. Hegazy^a, Sherry Lee^a, Fan Zhou^c, Nathan J. Sniadecki^{d,e,f}, Kathleen J. Green^{a,b,*}, and Horacio D. Espinosa^{c,g,*}

^aDepartment of Pathology and ^bDepartment of Dermatology, Feinberg School of Medicine, Northwestern University, Chicago, IL 60611; ^cDepartment of Mechanical Engineering and ^gTheoretical and Applied Mechanics Program, Northwestern University, Evanston, IL 60208; ^dDepartment of Mechanical Engineering, ^eDepartment of Bioengineering, and ^fInstitute for Stem Cell and Regenerative Medicine, University of Washington, Seattle, WA 98195

ABSTRACT The translation of mechanical forces into biochemical signals plays a central role in guiding normal physiological processes during tissue development and homeostasis. Interfering with this process contributes to cardiovascular disease, cancer progression, and inherited disorders. The actin-based cytoskeleton and its associated adherens junctions are well-established contributors to mechanosensing and transduction machinery; however, the role of the desmosome–intermediate filament (DSM–IF) network is poorly understood in this context. Because a force balance among different cytoskeletal systems is important to maintain normal tissue function, knowing the relative contributions of these structurally integrated systems to cell mechanics is critical. Here we modulated the interaction between DSMs and IFs using mutant forms of desmoplakin, the protein bridging these structures. Using micropillar arrays and atomic force microscopy, we demonstrate that strengthening the DSM–IF interaction increases cell–substrate and cell–cell forces and cell stiffness both in cell pairs and sheets of cells. In contrast, disrupting the interaction leads to a decrease in these forces. These alterations in cell mechanics are abrogated when the actin cytoskeleton is dismantled. These data suggest that the tissue-specific variability in DSM–IF network composition provides an opportunity to differentially regulate tissue mechanics by balancing and tuning forces among cytoskeletal systems.

Monitoring Editor
Asma Nusrat
Emory University

Received: Jul 18, 2016
Revised: Mar 16, 2017
Accepted: May 2, 2017

INTRODUCTION

Cells are integrated into tissues through macromolecular adhesive organelles specialized for anchoring different cytoskeletal compo-

nents at cell–extracellular matrix and cell–cell adhesion sites. At the cell substrate, actin and intermediate filaments (IFs) are anchored by focal adhesions and hemidesmosomes, respectively, whereas at cell–cell interfaces, actin and IFs are anchored by adherens junctions (AJs) and desmosomes (DSMs) (Simpson *et al.*, 2011). Under physiological conditions, these adhesion/cytoskeletal systems are highly integrated, and mechanical forces produced by individual cells are disseminated throughout a tissue by means of this cohesive network. The resulting mechanochemical coupling is required for tissue morphogenesis, collective cell migration, and cell proliferation and differentiation (DuFort *et al.*, 2011; Eyckmans *et al.*, 2011). Moreover, a number of pathological conditions and developmental disorders result from aberrant mechanical cues, including arthritis, atherosclerosis, and cancer (Jaalouk and Lammerding, 2009).

Cells within tissues exist in a “prestressed” condition, in which forces present within their mechanical components are balanced in a state of isometric tension; this has been suggested to be critical for mechanotransduction whereby mechanical forces are translated into biochemical cues (Ingber, 2008). Studies of mechanotransduction have focused primarily on actin-based adhesive organelles. For example, enhanced integrin signaling, resulting from matrix stiffening,

This article was published online ahead of print in MBoc in Press (<http://www.molbiolcell.org/cgi/doi/10.1091/mbc.E16-07-0520>) on May 11, 2017.

[†]These authors contributed equally.

Present addresses: [‡]Department of Mechanical and Materials Engineering, University of Nebraska-Lincoln, Lincoln, NE 68588; [§]Department of Biomedical Engineering, Carnegie Mellon University, Pittsburgh, PA 15213; ^{||}Department of Materials Science and Engineering, Pennsylvania State University, University Park, PA 16802.

*Address correspondence to: Kathleen J. Green (kgreen@northwestern.edu) or Horacio D. Espinosa (espinosa@northwestern.edu).

Abbreviations used: AFM, atomic force microscopy; AJ, adherens junction; CytoD, cytochalasin D; DMSO, dimethyl sulfoxide; DP, desmoplakin; DPNTF, desmoplakin N-terminal polypeptide; DRIE, deep reactive ion etching; DSM, desmosome; FOTS, tridecafluoro-(1,1,2,2)-tetrahydrooctyl trichlorosilane; GFP, green fluorescent protein; IF, intermediate filament; IgG, immunoglobulin G; MA, micropillar arrays; PBS, phosphate-buffered saline; PDMS, polydimethylsiloxane; siRNA, small interfering RNA; TCA, trichloroacetic acid; Wt, wild type.

© 2017 Broussard, Yang, *et al.* This article is distributed by The American Society for Cell Biology under license from the author(s). Two months after publication it is available to the public under an Attribution–Noncommercial–Share Alike 3.0 Unported Creative Commons License (<http://creativecommons.org/licenses/by-nc-sa/3.0/>).

“ASCB®,” “The American Society for Cell Biology®,” and “Molecular Biology of the Cell®” are registered trademarks of The American Society for Cell Biology.

promotes tumor progression (Levental *et al.*, 2009), and mechanical tension regulates Yap and β -catenin transcriptional activity through E-cadherin, driving cell cycle entry (Benham-Pyle *et al.*, 2015). Actomyosin contraction is required to generate tension at both cell–cell and cell–substrate adhesions (Aguilar-Cuenca *et al.*, 2014; de Rooij, 2014), and there is cross-talk between the mechanical forces at these two interfaces (Maruthamuthu *et al.*, 2011; Mertz *et al.*, 2013; Green *et al.*, 2015). In addition, actin-based AJs have an established role in regulating the emergence of tissue-level tension in cell monolayers (Harris *et al.*, 2014). However, much less is known about the role of the IF-based adhesions in regulating cell–cell and cell–substrate forces. In spite of their well-accepted role in maintaining the mechanical integrity of tissues, IF-based adhesions have been largely ignored with respect to their potential roles in mechanotransduction. Furthermore, though some progress has been made identifying how specific components of the mechanical networks participate in mechanotransduction, how these systems function cooperatively to orchestrate mechanically regulated cell behaviors remains poorly understood.

DSMs are cadherin-based cell adhesions that anchor strain-bearing IFs at sites of cell–cell contact (Figure 1A). They are the most prevalent adhesive structure in tissues that undergo considerable mechanical strain, including heart and skin, and DSM perturbations are associated with diseases of these organs (Broussard *et al.*, 2015). We have previously shown that enhancing or disrupting the connection

between DSMs and IFs qualitatively increases or decreases cell–cell adhesive strength (Bornslaeger *et al.*, 1996; Huen *et al.*, 2002; Hobbs and Green, 2012). However, the contribution of IF-based adhesive networks to cell–cell and cell–substrate forces and tissue-level tension is poorly understood.

Several methods for quantitative assessment of cell forces have been developed, including atomic force microscopy (AFM) (Brunner *et al.*, 2006; Prass *et al.*, 2006), traction force microscopy (Maruthamuthu *et al.*, 2011; Legant *et al.*, 2013; Benham-Pyle *et al.*, 2015), fluorescence microscopy–based tension biosensors (Grashoff *et al.*, 2010; Borghi *et al.*, 2012), optical traps (Galbraith and Sheetz, 1999; Kress *et al.*, 2007), and elastic micropillar arrays (MA) (Tan *et al.*, 2003; Liu *et al.*, 2010; Cohen *et al.*, 2013). These techniques have been used to study cell forces in the context of actin-based adhesive networks but have not been systematically applied to the study of IF-based adhesive networks. Here we use both MA and AFM to determine for the first time the contribution of the DSM–IF network to cell stiffness and cell–substrate and cell–cell mechanical forces. We demonstrate that modulating the strength of the DSM–IF linkage affects cell forces in the context of cell pairs and within larger groups of cells. In addition, our data show that these effects are at least in part mediated through regulation of the actin cytoskeleton and support a model in which the DSM–IF network could act as a compressive element, counterbalancing actomyosin-generated tension.

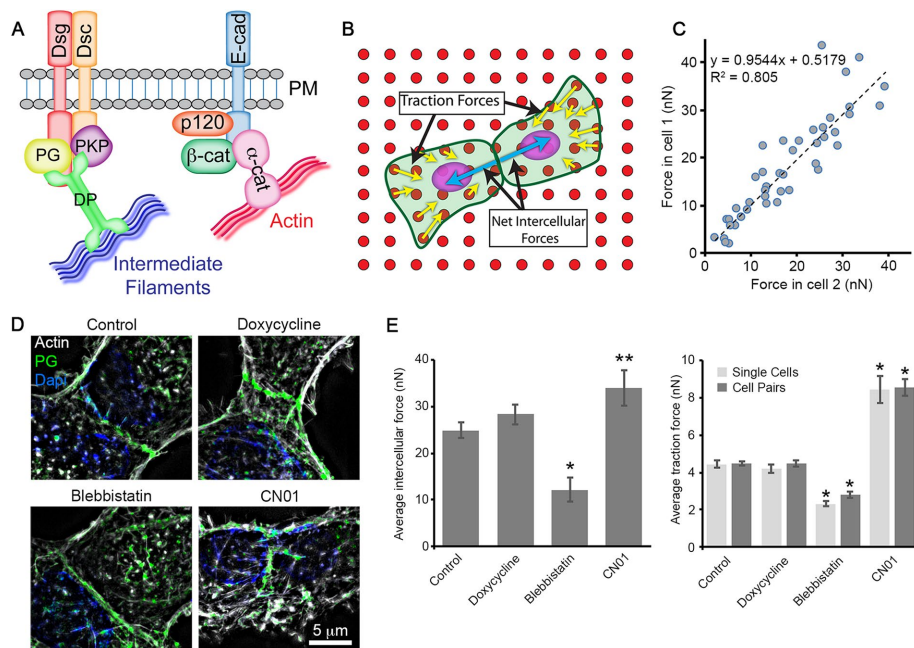


FIGURE 1: Quantification of cell–substrate and cell–cell adhesion using MA. (A) Schematic representation of the major protein constituents of DSMs (left) and AJs (right): PM, plasma membrane; DP, desmoglein; Dsg, desmocollin; PKP, plakophilin; PG, plakoglobin; E-cad, E-cadherin; p120, p120 catenin; β -cat, β -catenin; and α -cat, α -catenin. (B) Schematic representation of forces measured with MA. Cells (green) displace pillar tips (red) through traction forces (yellow arrows). Within cell pairs, the sum of the traction forces can be used to quantify net intercellular forces (blue arrows), which are equal and opposite in magnitude. (C) Force balance between cell pairs. The dashed line represents a linear regression, and the corresponding equation is shown. The theoretical condition in which the force in cell 1 equals the force in cell 2 would have a slope $m = 1$. (D) Superresolution micrographs of cells treated with the indicated compounds are shown with actin in white, plakoglobin (PG) in green to indicate the cell–cell junction, and DAPI in blue to show nuclei. (E) The average intercellular force and the average traction force per pillar are shown for cells treated with the indicated compounds. Error bars represent the standard error of the mean for 7–28 cells from three independent experiments. *, $p < 0.001$; **, $p = 0.02$.

RESULTS AND DISCUSSION

Measuring changes in contractility using MA

Modulating actomyosin contractility has previously been shown to regulate cell forces using MA (Liu *et al.*, 2010). This approach provided us a baseline with which to compare the role of the DSM–IF linkage in regulating cell forces as well as a means of validating our MA system. We generated MA using a process previously described (Yang *et al.*, 2011). Individual pillars had a height of 10 μ m and a diameter of 2 μ m (Supplemental Figure 1A). This resulted in a Young's modulus, as measured by AFM, of 2.41 ± 0.04 MPa. A mixture of fibronectin and fluorescent antibody was transferred onto the tips of the pillars by stamping, enabling cell attachment and pillar tip positioning to quantify displacement (Figure 1B). Cell forces deflect the pillars and can be measured by calculating the pillar displacement compared with a reference position obtained by interpolating the coordinates of unoccupied pillars. Traction forces are then calculated using the measured deflection, considering each pillar as an individual linear elastic mechanical cantilever beam with a tilted base (Schoen *et al.*, 2010; Yang *et al.*, 2011). To account for nonlinearity at large deflections, we performed finite element simulations to extract the traction force–displacement relationship of the pillars (Supplemental Figure 1, B and C). A quadratic function was obtained to calculate

cell forces: $f_i = 0.1921s_i^2 + 5.3659s_i$, where f_i and s_i are the traction force (nN) and lateral deflection of the pillar i (μm), respectively. Within a cell pair, the net forces are in equilibrium. Therefore the sum of the traction forces in one cell is equal and opposite in direction to that of the adjacent cell and vice versa, and thus represents the intercellular force (Liu *et al.*, 2010; Cohen *et al.*, 2013). This force balance was experimentally verified in our system (Figure 1C).

To determine whether our system is capable of detecting changes in cell forces, we either inhibited or enhanced cell contractility using the myosin inhibitor blebbistatin or the Rho activator CN01, respectively, and quantified intercellular forces in pairs of epidermoid carcinoma A431 cells and traction forces in cell pairs and individual cells. Cell pairs treated with these drugs retained cell-cell

contacts and intact actin cytoskeletons (Figure 1D). Blebbistatin led to a significant decrease in the average intercellular tugging force and traction force per pillar (Figure 1E), consistent with a report in endothelial cells (Liu *et al.*, 2010). Decreased cell-substrate forces were observed for both cell pairs and individual cells. However, CN01 resulted in a significant increase in these forces compared with dimethyl sulfoxide (DMSO)-treated controls (Figure 1E). These data suggest that quantification using our MA system is capable of detecting changes in cell-substrate and cell-cell adhesion forces.

The DSM-IF linkage regulates cell forces

To investigate the functional role of the DSM-IF network in regulating cell adhesive forces, we used inducible A431 stable cell lines

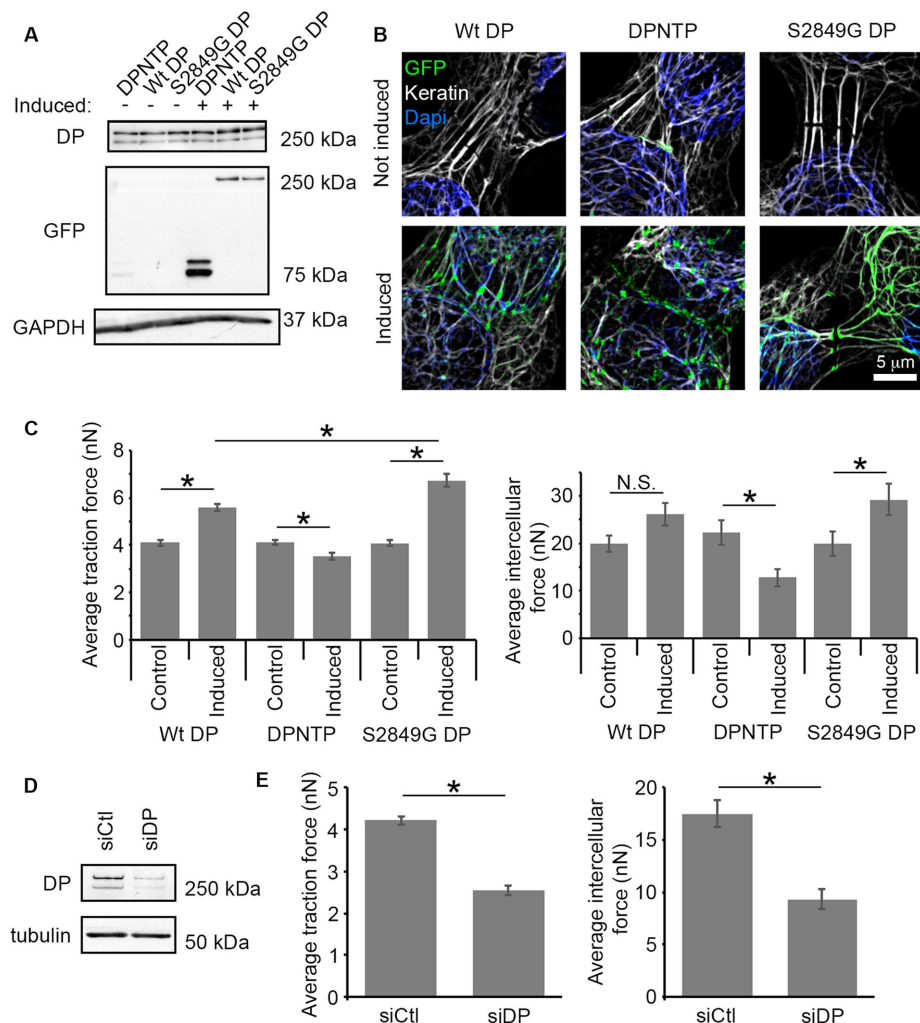


FIGURE 2: Modulating the DSM-IF connection leads to alterations in cell traction and tugging forces. (A) Western blot showing the expression of endogenous DP and doxycycline-induced expression of GFP-tagged DP variants. GAPDH is shown as a loading control. (B) Superresolution micrographs of control cells (not induced) and cells induced to express GFP-tagged DP variants are shown. The GFP-tagged DP variants are shown in green, keratin IFs are shown in white, and DAPI indicates nuclei in blue. (C) The average traction force per pillar and the average intercellular force are shown for control cells and cells induced to express the indicated DP variants. Error bars represent the standard error of the mean from at least 18 cells from three independent experiments. *, $p < 0.05$; N.S., not significant. (D) Representative Western blot indicating knockdown of endogenous DP in cells treated with either nontargeting siRNA (siCtl) or siRNA targeting DP (siDP). Tubulin is shown as a loading control. (E) The average traction force per pillar and the average intercellular force are shown for cells treated with either nontargeting siRNA (siCtl) or siRNA targeting DP (siDP). Error bars represent the standard error of the mean from at least 30 cells from three independent experiments. *, $p < 0.0001$.

expressing various forms of desmoplakin (DP), which provides the physical linkage from the DSM core components to IFs. These included wild type (Wt) DP, DPNTP, and S2849G DP (Figure 2A). Doxycycline, which is used to induce protein expression in this cell system, did not affect cell forces (Figure 1E). DPNTP is a DP truncation mutant lacking the IF-binding region of DP and uncouples DSMs from IFs (Bornslaeger *et al.*, 1996; Huen *et al.*, 2002; Figure 2B), while S2849G DP contains a serine to glycine mutation that enhances IF binding by interfering with GSK3 β -dependent processive phosphorylation of DP (Meng *et al.*, 1997; Hobbs and Green, 2012; Albrecht *et al.*, 2015; Figure 2B). Qualitatively, these mutations have been shown to decrease or increase cell-cell adhesion, respectively, but quantitative analysis has not been performed. In addition, the role of DP in regulating cell-substrate adhesion has not been addressed.

To determine whether modulating the DSM-IF linkage influences cell mechanics, we compared cell forces in control and DP variant-expressing cell pairs. Expression of DPNTP resulted in a decrease in the average intercellular tugging force and traction force per pillar compared with uninduced controls (Figure 2C). In addition, small interfering RNA (siRNA) targeting endogenous DP was used to knock down DP expression (Figure 2D). DP knockdown produced effects similar to those of DPNTP when compared with nontargeting siRNA controls (Figure 2E). These data suggest that uncoupling the DSMs from the IFs reduces both cell-cell and cell-substrate forces. Notably, DP knockdown resulted in a greater decrease in the average traction force per pillar compared with DPNTP. Because DPNTP displaces endogenous DP from cell-cell contacts but does not alter DP protein levels (Figure 2A), these data raise the possibility that nonjunctional DP impacts cell-substrate forces, perhaps indirectly through its ability to interact with other proteins, including kinases (Albrecht *et al.*, 2015). In contrast to

DPNTP, expression of S2849G DP resulted in a significant increase in cell forces when compared with controls (Figure 2C), suggesting increased DP interaction with IFs enhances cell forces. Notably, expression of Wt DP alone led to a significant increase in the average traction force per pillar (Figure 2C), though to a significantly lesser extent than in S2849G DP. We also observed a measurable, albeit not statistically significant, increase in the average intercellular tugging force upon expression of Wt DP (Figure 2C). These data suggest that enhancing the interaction between DSMs and IFs results in an increase in cell forces. Furthermore, they suggest that the cell mechanical network is not saturated under normal conditions, and potentially there is room within the system to modulate mechanical properties through increasing or decreasing the levels of Wt protein.

Alterations in intercellular forces do not generate corresponding changes in AJ tension as detected by the α -catenin α 18 epitope

Intercellular forces are transmitted cooperatively through the collective cell–cell adhesive organelles, including DSMs and AJs (Bazellieres *et al.*, 2015). To determine whether the changes in intercellular tugging forces observed downstream of DSM–IF modulation affected force within AJs, we employed an antibody (α 18) specific for the open conformation of α -catenin, the molecular link between AJs and the actin cytoskeleton (Figure 1A), which has been previously used to assess AJ tension (Yonemura *et al.*, 2010). Uncoupling the DSM–IF linkage by DPNTP expression led to an increase in α 18 staining, while there were no notable changes in total α -catenin (Supplemental Figure 2A). This resulted in an increased ratio of α 18 to total α -catenin (Supplemental Figure 2, B and C). One interpretation of these data is that AJs are under more tension upon DPNTP expression, which would be consistent with the previous observation that loss of DP increased markers of tension within AJs (Sumigay *et al.*, 2014). However, a recent study demonstrated that AJ protein clustering can induce α -catenin to enter an activated/open conformation, exposing the α 18 epitope, even in the absence of force (Biswas *et al.*, 2016). Therefore it is plausible that the increase in α 18 staining observed upon expression of DPNTP, rather than being the result of increased force on α -catenin, could be the result of AJ clustering. To address this possibility, we analyzed the distribution of α -catenin using object segmentation analysis. DPNTP expression resulted in an increased number of smaller α -catenin stained clusters with increased fluorescence intensity (Supplemental Figure 2, D and E). Considering the decreased cell–cell forces measured with MA when DPNTP is expressed, our data are consistent with the possibility that DPNTP expression exposes the α 18 epitope in α -catenin through a protein clustering–mediated conformational change, rather than an increase in AJ tension.

In addition, expression of Wt DP or S2849G DP had no effect on the ratio of α 18 to total α -catenin (Supplemental Figure 2C), indicating that the S2849G DP–mediated effects on average intercellular tugging force are not likely facilitated through increased forces or clustering, within AJs. It is also plausible that α -catenin already exists in a conformation that exceeds the unfolding threshold, precluding detection of additional tension downstream of DP modulation. Together, these data suggest that the observed effects on intercellular tugging forces observed downstream of DSM–IF modulation cannot be attributed solely to alterations in actin-based AJ forces.

The DSM–IF linkage regulates cell stiffness

To complement the results obtained using the MA and to extend them to groups of cells larger than pairs, we performed AFM cell stiffness measurements on single cells, cell pairs, and cell sheets.

AFM load-displacement measurements were performed by loading cells at their centroids (Figure 3, A and B). Whole-cell stiffness was computed from the acquired load-deflection curves (Figure 3B). Comparisons of control and DP variant–expressing cells did not reveal stiffness changes in single-cell measurements (Figure 3C). In cell pairs, the cell stiffness increased significantly upon expression of both Wt DP and S2849G DP (Figure 3C). However, expression of DPNTP and DP knockdown resulted in a significant decrease in the stiffness of cell pairs (Figure 3C). These results indicate that the DP-mediated alterations in cell forces observed using the MA are associated with corresponding changes in overall cell stiffness and are consistent with previous observations relating adherent and intercellular forces with overall levels of tension within the cytoskeleton (Ramms *et al.*, 2013; Selmann *et al.*, 2013).

To assess the role of the DSM–IF network during the later stages of monolayer sheet formation, we used AFM to measure the effects of DP modulation on semiconfluent cell sheets 2 d after seeding. For all controls, cell stiffness increased as a function of confluence (Figure 3, C and D), suggesting increased cell–cell adhesion promotes mechanical stiffening. In addition, uncoupling the DSM–IF linkage using DPNTP or DP siRNA in sheets of cells led to a significant decrease in cell stiffness compared with controls (Figure 3, D and E). In contrast, expression of S2849G DP led to a marked increase in cell stiffness in semiconfluent cell sheets (Figure 3D), while Wt DP had no effect.

It has been previously demonstrated that expression of S2849G DP in A431 cells promotes a calcium-independent, strongly adhesive state (Hobbs and Green, 2012), whereby cell sheets expressing this mutant have enhanced resistance to shear stress–induced fragmentation compared with Wt DP. Because both Wt DP and S2849G DP increase cell forces and cell stiffness, we assessed their contributions to cell stiffness in 6-d confluent sheets, for which differences in shear fragmentation were previously reported (Hobbs and Green, 2012). AFM measurements showed that Wt DP and S2849G DP expression both led to significant increases in cell stiffness in 6-d confluent cell sheets, with S2849G DP inducing a significantly larger increase (Figure 3F). These data are in agreement with the MA and AFM results on cell pairs and subconfluent sheets and the fragmentation data showing that enhanced IF binding properties of S2849G DP are associated with a more physically resistive state.

AFM can be used to assess the overall stiffness of an entire cell as well as to probe mechanical alterations at a subcellular level. Therefore AFM was used to examine the mechanical properties of cytoskeletal bundles near cell–cell adhesive interfaces for cell pairs in which the DSM–IF linkage was modulated (Supplemental Figure 3A, arrows). Superresolution imaging of these bundles demonstrate their attachment to sites of cell–cell adhesion at an orthogonal angle, an orientation normally observed for IFs and not actin or microtubules (Supplemental Figure 3B). An AFM tip was used to deflect individual cytoskeletal bundles near cell–cell junctions up to a load of 0.5 nN. The maximum deflection of the tip was then used to characterize stiffness. Expression of S2849G DP and Wt DP led to a significant reduction in the measured deflections (Supplemental Figure 3C), indicating elevated stiffness of the cytoskeletal bundles. The elevation could result from an increased amount of ectopic DP expression at sites of cell–cell contact providing an increased number of IF binding sites and thus enhancing the ability of IFs to resist AFM tip deflection. On the other hand, there were no differences detected upon expression of DPNTP (Supplemental Figure 3C). This suggests that, while DPNTP led to retraction of the majority of IFs from cell–cell junctions and an overall reduction in DSMs interacting with IFs (Supplemental Figure 4), the few DSM–IF connections that

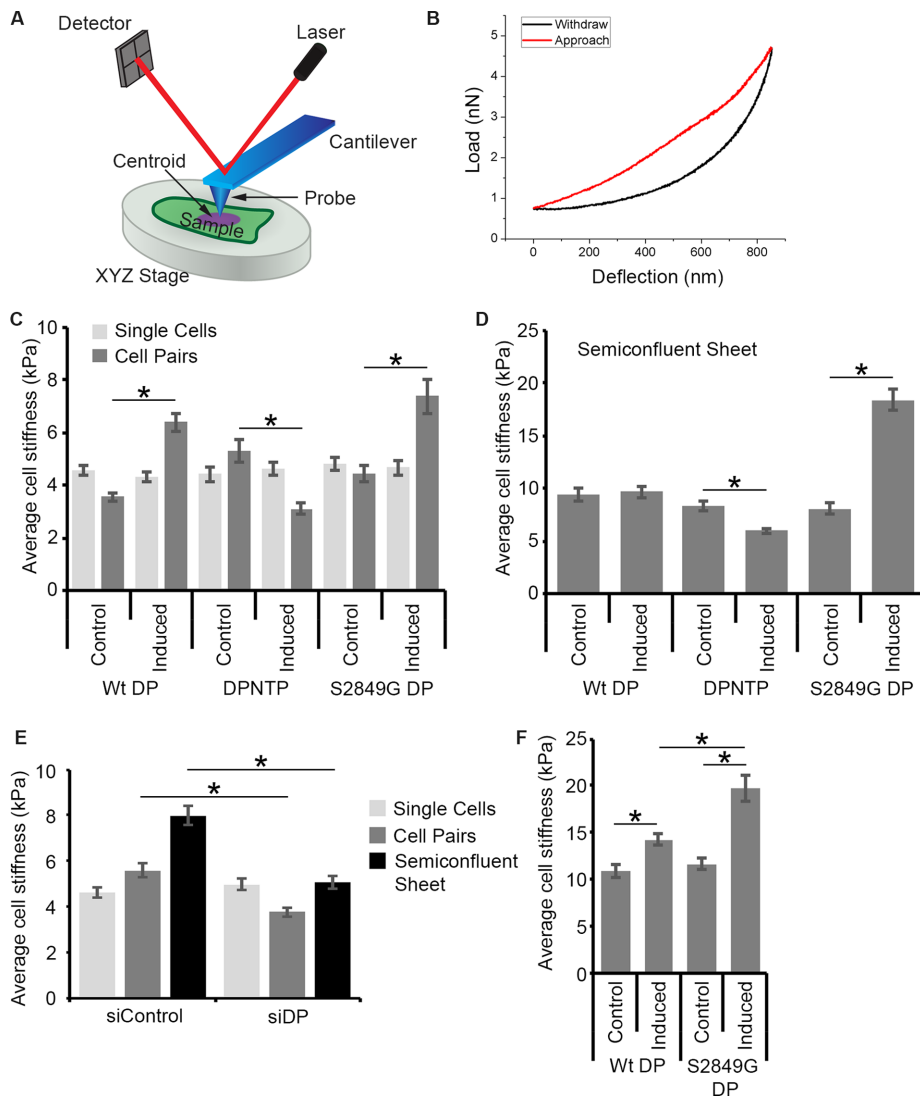


FIGURE 3: The DSM-IF network regulates cell stiffness. (A) Schematic diagram of an atomic force microscope. A cantilever is used to probe the physical properties of a cell. The displacement of the cantilever is determined by the movement of a laser across a detector. (B) A load vs. deflection function for both the approach and withdrawal of the AFM tip is shown. (C) Average cell stiffness measurements on single cells and cell pairs for cells expressing the indicated DP variants are shown (control and induced conditions). All force-displacement curves were taken by AFM on the cell centroid and were converted to stiffness using the Hertz model. Error bars represent the standard error of the mean from at least 45 cells from three independent experiments. *, $p < 0.0001$. (D) Average cell stiffness measurements of individual cells within semiconfluent (80%) cell sheets for cells expressing the indicated DP variants are shown (control and induced conditions). Error bars represent the standard error of the mean from at least 91 cells from three independent experiments. *, $p < 0.0001$. (E) Average cell stiffness measurements on single cells, cell pairs, and cell sheets for DP knockdown (siDP) and nontargeting siRNA control (siCt) conditions are shown. Error bars represent the standard error of the mean from at least 55 cells from three independent experiments. *, $p < 0.0001$. (F) Average cell stiffness measurements of calcium-insensitive, confluent cell sheets for cells expressing the indicated DP variants are shown. Error bars represent the standard error of the mean from at least 58 cells from three independent experiments. *, $p \leq 0.0002$.

do form have mechanical properties similar to those of controls, likely resulting from having similar levels of endogenous junctional DP. Note that the modest decrease in cytoskeletal bundles in S2849G DP-expressing cells could arise from increased IF bundling via the previously described retention of tightly bound S2849G DP along IFs in the cytoplasm (Godsel et al., 2005), where it could act as a cross-linker.

DSM-IF-mediated alterations in cell stiffness are dependent on actin

Because actomyosin contractility has been heavily implicated in the regulation of cell forces, we next asked whether DSM-IF modulation affected actin-related signaling. Rho is a major regulator of actomyosin signaling (Kimura et al., 1996). Therefore we examined the distribution of Rho in semiconfluent cell sheets, using a fixation method (Yonemura et al., 2004) that reveals increased Rho recruitment to lateral membranes upon activation (Figure 4, A–C) and staining cells with an antibody specific for active Rho bound to GTP (Figure 4, B and C). Treatment of cells with the Rho activator CN01 resulted in a significant cortical enrichment of Rho immunostaining compared with DMSO controls (Figure 4B). DPNTP expression led to a decrease in the cortical enrichment of Rho, while Wt DP and S2849G DP had no detectable effects (Figure 4C). Additionally, expression of DPNTP led to a decrease in cortical filamentous actin (F-actin) at cell–cell interfaces and a decrease in the average intensity of myosin IIa on cortical F-actin (Figure 4, D and E), while total myosin IIa protein levels did not change (Figure 4F). In contrast, we were unable to detect changes in Rho, F-actin, or myosin IIa upon expression of S2849G DP. These data suggest that uncoupling the DSM-IF linkage interferes with the junctional distribution and/or activation of Rho and the distribution of the actomyosin machinery.

The observed alterations in Rho, F-actin, and myosin IIa in DPNTP-expressing cells raised the possibility that the effects of DP modulation on cell stiffness in semiconfluent cell sheets involved the actin cytoskeleton. While changes were not detected in S2849G DP-expressing cells, this did not rule out a role for actin in affecting the increased stiffness observed in these cells. Toward directly addressing a role for actin, multiple concentrations of the actin disrupting drug cytochalasin D (CytoD) were used to destabilize the actin network in semiconfluent A431 cells (Figure 5A). DSMs appeared to still be present at all dosages, as assessed by a “railroad” pattern of cytoplasmic plaque DP staining at cell–cell contacts (Figure 5B; Chen et al., 2012). Destabilization of the actin network led to a dose-dependent decrease in cell stiffness (Figure 5C). Because the highest concentration of CytoD used (2.5 μ M) led to an almost complete loss of F-actin (Figure 5A), the middle (250 nM) and low (50 nM) doses were used to assess the involvement of the actin network downstream of DSM-IF modulation. When induced A431 cell lines were treated with 250 nM CytoD, Wt DP, DPNTP, and S2849G DP localized to cell–cell junctions, and Wt DP and S2849G DP exhibited a “railroad” pattern

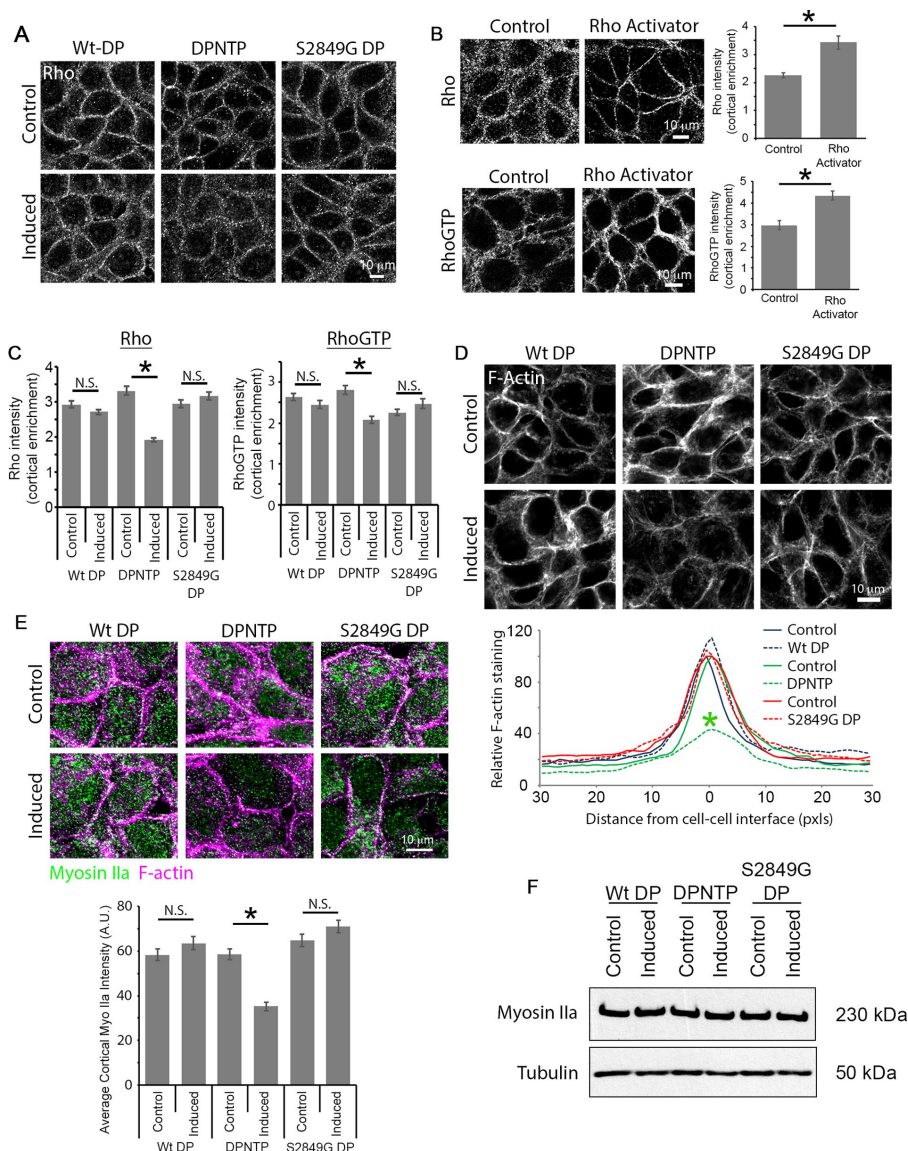


FIGURE 4: Disrupting the DSM–IF connection affects Rho, F-actin, and myosin IIa distribution. (A) Confocal micrographs of Rho immunostaining in control cells (not induced) and cells induced to express GFP-tagged DP variants and fixed with 10% TCA are shown. (B) Confocal micrographs of cells treated with the Rho activator CN01 and immunostained with a total Rho (fixed with 10% TCA) or a RhoGTP (fixed with 4% paraformaldehyde) antibody are shown. Control cells were treated with DMSO. Right, quantification of the cortical enrichment (cortical to noncortical ratio) of the indicated immunostaining is shown. Error bars represent the standard error of the mean from at least 30 cells from three independent experiments. *, $p < 0.0001$. (C) Quantification of the cortical enrichment (cortical to noncortical ratio) of total Rho and RhoGTP for control cells (not induced) and cells induced to express GFP-tagged DP variants are shown. Error bars represent the standard error of the mean from at least 50 cells from three independent experiments. *, $p < 0.0001$; N.S., not significant. (D) Confocal micrographs of phalloidin staining (F-actin) in control cells (uninduced) and cells induced to express GFP-tagged DP variants are shown. Right, line-scan analysis of the intensity of phalloidin staining as a function of distance from cell–cell interfaces for uninduced cells (Control) and cells induced to express the indicated GFP-tagged DP variants is shown. Green asterisk denotes significant difference upon expression of DPNT; *, $p = 0.0005$ from 20 cells from three independent experiments. (E) Apotome micrographs of control cells (not induced) and cells induced to express GFP-tagged DP variants that were stained with phalloidin (F-actin) and myosin IIa are shown. Below, quantification of the average intensity of myosin IIa on cortical F-actin in control cells (uninduced) and cells induced to express GFP-tagged DP variants is shown. Error bars represent the standard error of the mean from at least 55 cells from three independent experiments. *, $p < 0.0001$; N.S., not significant. (F) Representative Western blot indicating the level of myosin IIa in the indicated cells. Tubulin is shown as a loading control.

(Figure 5D), suggesting maintenance of the structural integrity of DSMs. The effects of both DPNT and S2849G DP expression on cell stiffness were abrogated by destabilizing the actin network using both the middle and low doses of CytoD (Figure 5E).

Collectively these data demonstrate that changes in cell forces due to modulation of the DSM–IF network are strongly dependent on the actin cytoskeleton. In the case of IF uncoupling through expression of DPNT, interference with junctional Rho may contribute to the observed changes. While we cannot rule out that changes in Rho occurred in S2849G DP–expressing cells that were not detected in our assays, other pathways such as actin bundling, cortical stiffening (e.g., ezrin, radixin, and moesin), or kinase signaling linked to DP may also be involved in governing the observed alterations in cell mechanics (Tseng et al., 2005; Fehon et al., 2010; Albrecht et al., 2015).

Our work is consistent with the following model. Under isometric tension, cells contain tensile elements and compressive elements. While the tensile component is widely thought to comprise the actomyosin machinery (Ingber, 2008), our data support the DSM–IF network functioning as a compressive element, resisting tension generated by actomyosin. Recently it has been suggested that keratin IFs can be under compressive forces (Nolting et al., 2014) and that vimentin IFs act to resist forces generated by actomyosin (Jiu et al., 2015). Therefore strengthening the DSM–IF network could increase the resistive capacity of the system by carrying greater compressive forces, allowing for more robust actomyosin-generated tension and increased cell forces/stiffness, while disruption would lead to the opposite effects (Figure 5F).

There are approximately 70 genes that encode IF products, some containing alternative splice forms, with similar structural organization but different primary amino acid sequences (Herrmann et al., 2009). Moreover, there are more than 10 genes encoding the core DSM components, some with multiple isoforms (Garrod and Chidgey, 2008). This provides an immense array of diversity within the composition of DSM–IF networks and potentially provides the capacity to finely tune mechanics based on tissue- and differentiation-dependent expression of these components. DSM–IF-mediated tuning of the mechanical force balance among the cytoskeletal systems is likely critical for regulating a cell's ability to respond to force stimuli and signal through mechanotransduction pathways.

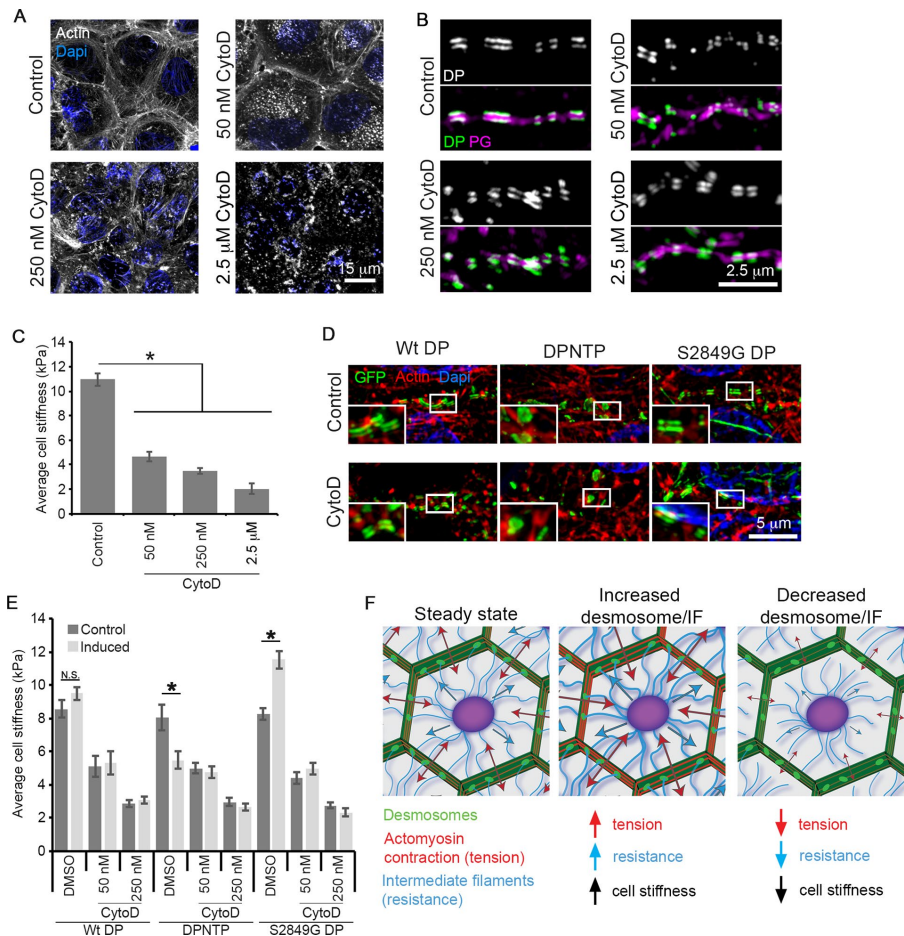


FIGURE 5: The DSM-IF-mediated effects on cell stiffness are dependent on the actin cytoskeleton. (A) Apotome micrographs of cells treated with the indicated concentrations of the actin depolymerization agent CytoD are shown with actin filaments (phalloidin staining) in white and DAPI in blue to show nuclei. DMSO was used as the control. (B) Superresolution micrographs of cells treated with the indicated concentrations of CytoD are shown with staining of DP in white (above) and in green (below) overlaid with plakoglobin (PG) in magenta at representative cell-cell junctions. DMSO was used as the control. (C) Average cell stiffness measurements of individual cells within semiconfluent (80%) cell sheets for cells treated with the indicated concentrations of CytoD are shown. DMSO was used as a control. Error bars represent the standard error of the mean from at least 99 cells from three independent experiments. *, $p < 0.0001$. (D) Superresolution micrographs of induced A431 cells expressing GFP-tagged DP variants and treated with 250 nM CytoD are shown. The GFP-tagged DP variants are shown in green, actin filaments (phalloidin staining) are shown in white, and DAPI indicates nuclei in blue. (E) Average cell stiffness measurements of individual induced or uninduced (control) A431 cells within semiconfluent (80%) cell sheets and treated with the indicated concentrations of CytoD or DMSO as a control are shown. Error bars represent the standard error of the mean from at least 30 cells from three independent experiments. *, $p < 0.01$; N.S., not significant. (F) Model: the DSM-IF linkage regulates the balance of cell forces. Cells exist in a "prestressed" state, which allows the system to respond rapidly to mechanical stimuli. There are tensile (red) and compressive (blue) elements that resist this tension. The tensile component is widely thought to be composed of the actomyosin machinery. Our data support a model in which the DSM-IF network may be functioning to resist the tension generated by actomyosin contractility. In this model, strengthening the DSM-IF connection leads to an increased resistive capacity of the system, allowing for more robust actomyosin-generated tension and increased cell forces/stiffness. However, uncoupling the DSM-IF network would decrease the resistive capacity and lead to a decrease in actomyosin-generated tension and cell forces/stiffness.

MATERIALS AND METHODS

Micropillar substrate fabrication and functionalization

Polydimethylsiloxane (PDMS) MA substrates were fabricated by following previously published protocols with some modifications. The patterns on a photomask were first transferred onto the photoresist

layer on a silicon wafer using conventional contact lithography. A silicon wafer spin coated with a uniform layer of 1.2- μm -thick photoresist S1813 was exposed to UV light in a MABA6 aligner (Karl Suss, Munich, Germany), which was followed by developing in the developer MF-351 solution. The patterned photoresist layer then served as the mask to pattern the silicon wafer using deep reactive ion etching (DRIE; STS LpX Pegasus). Silicon micropost arrays with a height of $\sim 10 \mu\text{m}$ were obtained after carefully controlled DRIE etching. Two sequential PDMS replica-molding steps were performed to obtain PDMS micropost arrays from the silicon micropost arrays. Before the first replica-molding step, the silicon mold was cleaned with oxygen plasma and then coated with a surfactant self-assembled monolayer, tridecafluoro-(1,1,2,2)-tetrahydrooctyl trichlorosilane (FOTS; Gelest) to lower surface energy. More specifically, the silicon wafer was immersed in a 0.5% wt solution of FOTS in heptane at 65°C for 5 min, which was followed by cleaning in pure heptane solution to remove redundant surfactant and 10 min baking at 100°C to improve the strength of the release layer. For making the PDMS negative mold, a mixture of elastomer and curing agent at a 10:1 ratio was poured onto the silicon mold, placed in a vacuum for 45 min, and heated to 100°C on a hot plate for 2 h. The PDMS was then peeled off the silicon mold, yielding the negative mold. The same surface treatment was performed on the negative mold before the second replica-molding step. The same PDMS solution used in the previous step was coated on each PDMS negative mold with a thickness of $\sim 2 \text{ mm}$. The coated molds were placed in a vacuum for at least 1 h to ensure that the liquid PDMS fully filled in the high aspect ratio holes without gas trapping. Then each PDMS mold was turned over and placed on a clean glass substrate and cured on a hot plate at 100°C for 2 h. The baking time was kept equal for all batches of samples to ensure consistent mechanical properties of the cured PDMS pillars. After immersion in isopropanol for at least 6 h, the PDMS MA were manually peeled off the negative mold. Finally, critical-point drying (Tousimis Automegasamdri-915B, Series C) was performed to remove the isopropanol without collapsing the pillars. The fabricated PDMS pillar arrays were characterized using scanning electron microscopy (FEI Nova 600) and a 3D profilometer (ZYGO).

Surface functionalization

PDMS stamps were prepared by curing the mixture of elastomer and curing agent at 15:1 ratio in a clean Petri dish and then cutting individual pieces of similar size to the MA substrate. After sequential cleaning in isopropanol and distilled water, a mixture of fibronectin

and Alex Fluor–conjugated immunoglobulin G (IgG) antibodies, at a weight ratio of 4:1 with a total weight concentration of 50 $\mu\text{g}/\text{ml}$, was pipetted onto the tops of PDMS stamps with the face in contact with the Petri dish bottom surface facing up. Excess solution was carefully removed using a Kimwipe after 1 h incubation at room temperature. The stamps were blow-dried with nitrogen. The MA substrates were treated with a UV-ozone cleaner (BioForce, Ames, IA) for 7 min. Immediately after the UV-ozone treatment, the stamps were flipped over to allow their top surfaces to make contact with the top of the MA and gently pressed with a tweezer. After the stamps were separated from the MA, the substrates were sterilized and rinsed by sequentially dipping the substrates into 100% isopropanol and 70% isopropanol, followed by distilled water for three times. The substrates were then incubated in 0.2% pluronics F-127 in phosphate-buffered saline (PBS) for 45 min at room temperature, which was followed by rinsing twice in sterile PBS.

Cell culture, pharmacological treatments, and RNAi

A431 cells were maintained in DMEM (Corning, Corning, NY) supplemented with 10% fetal bovine serum (Sigma-Aldrich, St. Louis, MO) and 1% penicillin–streptomycin (Corning) (growth medium) at 37°C with 5% CO_2 . Stable A431 cell lines were generated by transfecting parental cells with pTet-On (Clontech, Mountain View, CA), followed by selection with 400 $\mu\text{g}/\text{ml}$ G418 (Corning), and subsequently transfecting with pTRE (Clontech) plasmids expressing DPNTP–green fluorescent protein (GFP), DP-S2849G-GFP, or wild-type DP-GFP (Huen *et al.*, 2002; Godsel *et al.*, 2005). For induction, cells were cultured with 4 $\mu\text{g}/\text{ml}$ doxycycline (Sigma-Aldrich) in growth medium for 18 h. Subsequently both noninduced and induced cells were plated at low density onto MA and cultured overnight. Pharmacological treatments modulating cell contractility included 3 μM blebbistatin (Sigma-Aldrich) for 2 h and 1 unit/ml Rho Activator I (CN01; Cytoskeleton, Denver, CO) for 30 min. Parental A431 cells were transfected with either siGENOME Non-Targeting siRNA Pool #2 or siGENOME SMARTpool siRNA D-019800-17 DSP (Dharmacon, Lafayette, CO) using DharmaFECT (GE Healthcare, Pittsburgh, PA), according to the manufacturer's instructions.

Immunofluorescence, image acquisition, and image quantification

A431 cells cultured on either glass coverslips (VWR, Radnor, PA) or MA were rinsed with PBS, fixed in 4% paraformaldehyde for 10 min, with or without subsequent fixation using anhydrous methanol for 3 min, and processed for immunofluorescence. Trichloroacetic acid (TCA; Sigma-Aldrich) fixation for RhoA antibody staining was performed as previously described (Yonemura *et al.*, 2004). Primary antibodies included KSB 17.2 (Sigma-Aldrich), 1407 (Aves Labs, Tigard, OR), HECD-1 (a gift from Masatoshi Takeichi and Osahiko Abe, RIKEN Center for Developmental Biology, Kobe, Japan), 1G5 (a gift from the late Margaret Wheelock, University of Nebraska), α 18 (a gift from Akira Nagafuchi, Nara Medical University, Japan), DM1A (Sigma-Aldrich), myosin IIa antibody (Cell Signaling Technology, Danvers, MA), RhoA antibody (26C4; Santa Cruz Biotechnology, Dallas, TX), and anti-active RhoA mouse monoclonal antibody (RhoGTP; NewEast Biosciences, King of Prussia, PA). Secondary antibodies included Alexa Fluor 488–, 568–, and 647–conjugated anti-mouse, anti-rabbit, or anti-chicken IgG (Life Technologies, Grand Island, NY). Alexa Fluor 568 phalloidin (Life Technologies) was used to visualize filamentous actin.

Apotome images were acquired using an epifluorescence microscope system (AxioVision Z1; Carl Zeiss, Thornwood, NY) fitted with an Apotome slide module, AxioCam MRm digital camera, and a 40 \times /0.5 EC Plan-Neofluar or 100 \times /1.4 NA oil Plan-Apochromat ob-

jective (Carl Zeiss). Superresolution images were acquired using a Nikon TiE N-SIM system with a 100 \times objective lens (NA 1.40; Nikon, Tokyo, Japan) and an iXon X3 897 camera (Andor Technology, Belfast, United Kingdom). SIM images were reconstructed using NIS Elements version 4.20.01 software (Build 982; Nikon). Confocal images were acquired using a Nikon A1R confocal laser microscope equipped with GaAsP detectors and a 60 \times Plan-Apochromat objective lens with an NA of 1.4 and run by NIS Elements software (Nikon).

For quantifying the number of IF bundles attached at sites of cell–cell contact, immunofluorescence was used to visualize both keratin bundles (KSB 17.2) and cell junctions (PG, 1407). IF bundles entering perpendicular to the cell junctions were quantified with ImageJ software (National Institutes of Health). The number of IF bundles was divided by border length (in pixels) and then averaged for each condition. The average fluorescence intensity of total α -catenin (1G5), α 18, the ratio of α 18 to total α -catenin, the cortical to noncortical ratio of either total Rho or RhoGTP staining at cell–cell junctions, and myosin IIa staining on cortical actin (identified with phalloidin staining) were quantified using MetaMorph version 7.8.0.0 software (Molecular Devices, Sunnyvale, CA). A linescan analysis (5 pixels wide) of phalloidin (F-actin) staining at cell–cell junctions was performed using MetaMorph software. Object segmentation analysis of α -catenin staining was performed using the Integrated Morphometry Analysis function in MetaMorph to calculate the average object number, size, and intensity per cell–cell border. All image analysis experiments were performed for at least three independent experiments.

AFM imaging and force measurements

Control and induced A431 cells were cultured in growth medium at 37°C and 5% CO_2 for either 2 or 6 d before experiments. For siRNA knockdown, experiments were carried out 3 d after DharmaFECT transfection with siRNA (40 nM). For the actin depolymerization experiments, cells were incubated with CytoD (2.5 μM , 250 nM, or 50 nM) for 1 h at 37°C, and DMSO was used as a control. AFM imaging and force measurements of live cells were carried out in cell growth medium at 37°C using the Peakforce Tapping mode on a Catalyst AFM system (Bruker Nano, Santa Barbara, CA). A silicon nitride cantilever with a tip radius of \sim 20 nm and a nominal spring constant of 0.3 N/m (Bruker Nano), calibrated using the thermal tune method (Lévy and Maaloum, 2002), was used for force measurements. Both trace and retrace curves were analyzed. The approach speed was set at 0.5 $\mu\text{m}/\text{s}$ to reduce the effects of cell viscosity. Collected force curves were processed with a Matlab routine to convert them into stiffness values using the Sneddon model (Cappella and Dietler, 1999). The tip half opening angle was 17.5°, and the Poisson ratio was 0.5.

Statistical analysis

Statistical analyses were performed using an unpaired *t* test, and statistical significance was determined at $p < 0.05$.

ACKNOWLEDGMENTS

This work was supported by National Institutes of Health (NIH) grants from the National Institute of Arthritis and Musculoskeletal and Skin Diseases (AR042836 and AR043380) and the National Cancer Institute (NCI; CA122151). J.A.B. was supported by a Training Grant: Post Graduate Program in Cutaneous Biology (T32 AR060710). The authors acknowledge support from the McCormick School of Engineering through a catalyst award and the Chicago Biomedical Consortium with support from the Searle Funds at the Chicago Community Trust. Imaging work was performed at the Northwestern University Center for Advanced Microscopy

generously supported by NCI CCSG P30 CA060553 awarded to the Robert H. Lurie Comprehensive Cancer Center. Structured illumination microscopy was performed on a Nikon N-SIM system, purchased through the support of NIH 1S10OD016342-01.

REFERENCES

- Aguilar-Cuenca R, Juanes-García A, Vicente-Manzanares M (2014). Myosin II in mechanotransduction: master and commander of cell migration, morphogenesis, and cancer. *Cell Mol Life Sci* 71, 479–492.
- Albrecht LV, Zhang L, Shabanowitz J, Purejav E, Towbin JA, Hunt DF, Green KJ (2015). GSK3- and PRMT-1-dependent modifications of desmoplakin control desmoplakin-cytoskeleton dynamics. *J Cell Biol* 208, 597–612.
- Bazellieres E, Conte V, Elsegui-Artola A, Serra-Picamal X, Bintanel-Morcillo M, Roca-Cusachs P, Munoz JJ, Sales-Pardo M, Guimera R, Trepas X (2015). Control of cell-cell forces and collective cell dynamics by the intercellular adhesome. *Nat Cell Biol* 17, 409–420.
- Benham-Pyle BW, Pruitt BL, Nelson WJ (2015). Cell adhesion. Mechanical strain induces E-cadherin-dependent Yap1 and beta-catenin activation to drive cell cycle entry. *Science* 348, 1024–1027.
- Biswas KH, Hartman KL, Zaidel-Bar R, Groves JT (2016). Sustained alpha-catenin activation at E-cadherin junctions in the absence of mechanical force. *Biophys J* 111, 1044–1052.
- Borghi N, Sorokina M, Shcherbakova OG, Weis WI, Pruitt BL, Nelson WJ, Dunn AR (2012). E-cadherin is under constitutive actomyosin-generated tension that is increased at cell-cell contacts upon externally applied stretch. *Proc Natl Acad Sci USA* 109, 12568–12573.
- Bornslaeger EA, Corcoran CM, Stappenbeck TS, Green KJ (1996). Breaking the connection: displacement of the desmosomal plaque protein desmoplakin from cell-cell interfaces disrupts anchorage of intermediate filament bundles and alters intercellular junction assembly. *J Cell Biol* 134, 985–1001.
- Broussard JA, Getsios S, Green KJ (2015). Desmosome regulation and signaling in disease. *Cell Tissue Res* 360, 501–512.
- Brunner C, Ehrlicher A, Kohlstrunk B, Knebel D, Käs J, Goegler M (2006). Cell migration through small gaps. *Eur Biophys J* 35, 713–719.
- Cappella B, Dietler G (1999). Force-distance curves by atomic force microscopy. *Surf Sci Rep* 34, 1–104.
- Chen J, Nekrasova OE, Patel DM, Klessner JL, Godsel LM, Koetsier JL, Amargo EV, Desai BV, Green KJ (2012). The C-terminal unique region of desmoglein 2 inhibits its internalization via tail-tail interactions. *J Cell Biol* 199, 699–711.
- Cohen DM, Yang MT, Chen CS (2013). Measuring cell-cell tugging forces using bowtie-patterned mPADs (microarray post detectors). *Methods Mol Biol* 1066, 157–168.
- de Rooij J (2014). Cadherin adhesion controlled by cortical actin dynamics. *Nat Cell Biol* 16, 508–510.
- DuFort CC, Paszek MJ, Weaver VM (2011). Balancing forces: architectural control of mechanotransduction. *Nat Rev Mol Cell Biol* 12, 308–319.
- Eyckmans J, Boudou T, Yu X, Chen CS (2011). A hitchhiker's guide to mechanobiology. *Dev Cell* 21, 35–47.
- Fehon RG, McClatchey AI, Bretscher A (2010). Organizing the cell cortex: the role of ERM proteins. *Nat Rev Mol Cell Biol* 11, 276–287.
- Galbraith CG, Sheetz MP (1999). Keratocytes pull with similar forces on their dorsal and ventral surfaces. *J Cell Biol* 147, 1313–1324.
- Garrod D, Chidgey M (2008). Desmosome structure, composition and function. *Biochim Biophys Acta* 1778, 572–587.
- Godsel LM, Hsieh SN, Amargo EV, Bass AE, Pascoe-McGillicuddy LT, Huen AC, Thorne ME, Gaudry CA, Park JK, Myung K, et al. (2005). Desmoplakin assembly dynamics in four dimensions: multiple phases differentially regulated by intermediate filaments and actin. *J Cell Biol* 171, 1045–1059.
- Grashoff C, Hoffman BD, Brenner MD, Zhou R, Parsons M, Yang MT, McLean MA, Sligar SG, Chen CS, Ha T, Schwartz MA (2010). Measuring mechanical tension across vinculin reveals regulation of focal adhesion dynamics. *Nature* 466, 263–266.
- Green A, Green H, Rehnberg M, Svensson A, Gunnarsson C, Jonasson J (2015). Assessment of HaloPlex amplification for sequence capture and massively parallel sequencing of arrhythmogenic right ventricular cardiomyopathy-associated genes. *J Mol Diagn* 17, 31–42.
- Harris AR, Daeden A, Charras GT (2014). Formation of adherens junctions leads to the emergence of a tissue-level tension in epithelial monolayers. *J Cell Sci* 127, 2507–2517.
- Herrmann H, Strelkov SV, Burkhard P, Aebi U (2009). Intermediate filaments: primary determinants of cell architecture and plasticity. *J Clin Invest* 119, 1772–1783.
- Hobbs RP, Green KJ (2012). Desmoplakin regulates desmosome hyperadhesion. *J Invest Dermatol* 132, 482–485.
- Huen AC, Park JK, Godsel LM, Chen X, Bannon LJ, Amargo EV, Hudson TY, Mongiui AK, Leigh IM, Kelsell DP, et al. (2002). Intermediate filament-membrane attachments function synergistically with actin-dependent contacts to regulate intercellular adhesive strength. *J Cell Biol* 159, 1005–1017.
- Ingber DE (2008). Tensegrity-based mechanosensing from macro to micro. *Prog Biophys Mol Biol* 97, 163–179.
- Jaalouk DE, Lammerding J (2009). Mechanotransduction gone awry. *Nat Rev Mol Cell Biol* 10, 63–73.
- Jiu Y, Lehtimäki J, Tojkander S, Cheng F, Jaalinoja H, Liu X, Varjosalo M, Eriksson JE, Lappalainen P (2015). Bidirectional interplay between vimentin intermediate filaments and contractile actin stress fibers. *Cell Rep* 11, 1511–1518.
- Kimura K, Ito M, Amano M, Chihara K, Fukata Y, Nakafuku M, Yamamori B, Feng J, Nakano T, Okawa K, et al. (1996). Regulation of myosin phosphatase by Rho and Rho-associated kinase (Rho-kinase). *Science* 273, 245–248.
- Kress H, Stelzer EH, Holzer D, Buss F, Griffiths G, Rohrbach A (2007). Filopodia act as phagocytic tentacles and pull with discrete steps and a load-dependent velocity. *Proc Natl Acad Sci USA* 104, 11633–11638.
- Legat WR, Choi CK, Miller JS, Shao L, Gao L, Betzig E, Chen CS (2013). Multidimensional traction force microscopy reveals out-of-plane rotational moments about focal adhesions. *Proc Natl Acad Sci USA* 110, 881–886.
- Levental KR, Yu H, Kass L, Lakins JN, Egeblad M, Erler JT, Fong SF, Csiszar K, Giaccia A, Weninger W, et al. (2009). Matrix crosslinking forces tumor progression by enhancing integrin signaling. *Cell* 139, 891–906.
- Lévy R, Maaloum M (2002). Measuring the spring constant of atomic force microscope cantilevers: thermal fluctuations and other methods. *Nanotechnology* 13, 33.
- Liu Z, Tan JL, Cohen DM, Yang MT, Sniadecki NJ, Ruiz SA, Nelson CM, Chen CS (2010). Mechanical tugging force regulates the size of cell-cell junctions. *Proc Natl Acad Sci USA* 107, 9944–9949.
- Maruthamuthu V, Sabass B, Schwarz US, Gardel ML (2011). Cell-ECM traction force modulates endogenous tension at cell-cell contacts. *Proc Natl Acad Sci USA* 108, 4708–4713.
- Meng JJ, Bornslaeger EA, Green KJ, Steinert PM, Ip W (1997). Two-hybrid analysis reveals fundamental differences in direct interactions between desmoplakin and cell type-specific intermediate filaments. *J Biol Chem* 272, 21495–21503.
- Mertz AF, Che Y, Banerjee S, Goldstein JM, Rosowski KA, Revilla SF, Niessen CM, Marchetti MC, Dufresne ER, Horsley V (2013). Cadherin-based intercellular adhesions organize epithelial cell-matrix traction forces. *Proc Natl Acad Sci USA* 110, 842–847.
- Nolting JF, Mobius W, Koster S (2014). Mechanics of individual keratin bundles in living cells. *Biophys J* 107, 2693–2699.
- Prass M, Jacobson K, Mogilner A, Radmacher M (2006). Direct measurement of the lamellipodial protrusive force in a migrating cell. *J Cell Biol* 174, 767–772.
- Ramms L, Fabris G, Windoffer R, Schwarz N, Springer R, Zhou C, Lazar J, Stiefel S, Hersch N, Schnakenberg U, et al. (2013). Keratins as the main component for the mechanical integrity of keratinocytes. *Proc Natl Acad Sci USA* 110, 18513–18518.
- Schoen I, Hu W, Klotzsch E, Vogel V (2010). Probing cellular traction forces by micropillar arrays: contribution of substrate warping to pillar deflection. *Nano Lett* 10, 1823–1830.
- Selmann K, Fritsch AW, Kas JA, Magin TM (2013). Keratins significantly contribute to cell stiffness and impact invasive behavior. *Proc Natl Acad Sci USA* 110, 18507–18512.
- Simpson CL, Patel DM, Green KJ (2011). Deconstructing the skin: cytoarchitectural determinants of epidermal morphogenesis. *Nat Rev Mol Cell Biol* 12, 565–580.
- Sumigra K, Zhou K, Lechler T (2014). Cell-cell adhesions and cell contractility are upregulated upon desmosome disruption. *PLoS One* 9, e101824.
- Tan JL, Tien J, Pirone DM, Gray DS, Bhadriraju K, Chen CS (2003). Cells lying on a bed of microneedles: an approach to isolate mechanical force. *Proc Natl Acad Sci USA* 100, 1484–1489.
- Tseng Y, Kole TP, Lee JS, Fedorov E, Almo SC, Schafer BW, Wirtz D (2005). How actin crosslinking and bundling proteins cooperate to generate an enhanced cell mechanical response. *Biochem Biophys Res Commun* 334, 183–192.
- Yang MT, Fu J, Wang YK, Desai RA, Chen CS (2011). Assaying stem cell mechanobiology on microfabricated elastomeric substrates with geometrically modulated rigidity. *Nat Protoc* 6, 187–213.
- Yonemura S, Hirao-Minakuchi K, Nishimura Y (2004). Rho localization in cells and tissues. *Exp Cell Res* 295, 300–314.
- Yonemura S, Wada Y, Watanabe T, Nagafuchi A, Shibata M (2010). α -Catenin as a tension transducer that induces adherens junction development. *Nat Cell Biol* 12, 533–542.